ADVANCED MATERIALS
www.advmat.de

Ultimately Adaptive Fluid Interfacial Phospholipid Membranes Unveiled Unanticipated High Cellular Mechanical Work

*Zhou Lu, Mizuki Tenjimbayashi, Junhong Zhou, and Jun Nakanishi**

Living cells actively interact biochemically and mechanically with the surrounding extracellular matrices (ECMs) and undergo dramatic morphological and dimensional transitions, concomitantly remodeling ECMs. However, there is no suitable method to quantitatively discuss the contribution of mechanical interactions in such mutually adaptive processes. Herein, a highly deformable "living" cellular scaffold is developed to evaluate overall mechanical energy transfer between cell and ECMs. It is based on the water–perfluorocarbon interface decorated with phospholipids bearing a cell-adhesive ligand and fluorescent tag. The bioinert nature of the phospholipid membranes prevents the formation of solid-like protein nanofilms at the fluid interface, enabling to visualize and quantify cellular mechanical work against the ultimately adaptive model ECM. A new cellular wetting regime is identified, wherein interface deformation proceeds to cell flattening, followed by its eventual restoration. The cellular mechanical work during this adaptive wetting process is one order of magnitude higher than those reported with conventional elastic platforms. The behavior of viscous liquid drops at the air–water interface can simulate cellular adaptive wetting, suggesting that overall viscoelasticity of the cell body predominates the emergent wetting regime and regulates mechanical output. Cellular-force-driven high-energy states on the adaptive platform can be useful for cell fate manipulation.

1. Introduction

As a hallmark of living system, there is dynamic reciprocity between cells and the surrounding extracellular matrices (ECMs), through which they remodel each other biochemically and mechanically.[1] During this process, living cells undergo dramatic morphological and dimensional transitions, eventually regulating their own activities and fate.[2] Therefore, the methods for mimicking such "living" nature of cell–ECM interaction, either from the matrix and cellular sides, are critical not only for the fundamental understanding of the time-dependent responses, but also for producing medically useful cellular resources and synthetic biology.[3]

For example, in the mechanobiology field, it has become common to explain cell spreading process under the motor-clutch model framework, based on the dynamic engagement and disengagement of molecular clutches in actin retrograde flow.[4] By introducing the stress-relaxing property to hydrogels, the dynamic nature of the substrates has been shown to influence the cell spreading speed and force transmission, as well as stem cell differentiation.[5] Therefore, matching the material and cellular timescale is critical for biomaterial design.[6] On the other hand, from a physical viewpoint, there is an analogy between the wetting behavior of liquid drops and the spreading of cell aggregates onto 2D substrates.[7] The morphological transition of the aggregates is determined by the balance between cell–cell and cell–substrate adhesion energies. By introducing the chemically inducible E-cadherin expression system to epithelial cell monolayers, the concept has been further extended to "active wetting/dewetting" to include the

Z. Lu, J. Zhou, J. Nakanishi
Research Center for Macromolecules and Biomaterials
National Institute for Materials Science (NIMS)
1-1 Namiki, Tsukuba, Ibaraki 305-0044, Japan
E-mail: nakanishi.Jun@nims.go.jp

The ORCID identification number(s) for the author(s) of this article can be found under https://doi.org/10.1002/adma.202403396

DOI: 10.1002/adma.202403396

M. Tenjimbayashi
Research Center for Materials Nanoarchitectonics (MANA)
NIMS, 1-1 Namiki, Tsukuba, Ibaraki 305-0044, Japan

J. Zhou, J. Nakanishi
Graduate School of Advanced Science and Engineering
Waseda University
3-4-1 Okubo, Shinjuku-ku, Tokyo 169-8555, Japan

J. Nakanishi
Graduate School of Advanced Engineering
Tokyo University of Science
6-3-1 Niijuku, Katsushika-ku, Tokyo 125-8585, Japan

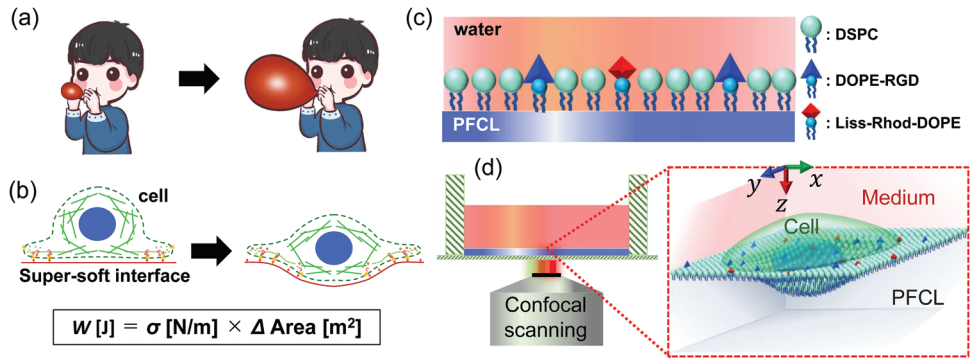

Figure 1. Concept of this study. a) Analogy between cell mechanical work measurement by the present methodology and spirometry measurement using a balloon. b) Cell traction force-driven deformation of the super-soft liquid interface. An equation to calculate mechanical energy transfer between the cell and model ECM from interfacial tension (σ) and area change. c) Coating the water–PFCL (perfluorocarbon liquid) interface with phospholipids bearing a cell-adhesive RGD peptide and a fluorescent tag (Liss-Rhod, lissamine rhodamine). d) Observation of cell and IPLM wetting process by confocal microscopy.

time-evolving nature of the cell–cell adhesion energy and subsequent wetting transition of cell clusters.[8] This study highlighted a significant role of dynamic mechanics changes in tissue morphogenesis and tumor progression.

However, it is still unclear how large the contribution of mechanical interactions is during the entire mutual adaptation process of the cell–ECM interactions, especially when both sides have "living" nature. This is because most conventional force detection methodologies either rely on the linear elastic nature of materials[9] or provide spatially limited information depending on the distribution of probe molecules.[10] In addition, conventional technologies focus on detecting in-plane forces (horizontal to the cell–ECM interface), whereas out-of-plane forces (vertical to the cell–ECM interface) are mostly neglected. Because of these reasons, it is almost impossible to quantitatively discuss overall mechanical energy transferred between cells and ECMs during their mutual adaptive responses. In this regard, fluids are supersoft, allowing to detect cellular mechanical forces nonexclusively, even for the extremely weak vertical component, and report them as interfacial strain. Moreover, by choosing a low viscous fluid, such as perfluorocarbon liquid (PFCL, $\eta = 10^{-3}$–10^{-2} Pa s), viscous energy dissipation becomes negligible, thereby the cellular mechanical work is efficiently transferred to the strain energy of the fluid interface. Therefore, in a similar fashion to the spirometry measurement using a balloon (**Figure 1a**), the mechanical work can be precisely calculated from the product of interfacial tension and the area increase of the fluid interface (Figure 1b). However, in normal cell culture conditions, proteins involved in the aqueous media assemble at the liquid–liquid interfaces to form robust solid-like proteinaceous nanolayers to lower interfacial energy.[11] The formation of the robust protein nanolayers is advantageous for sustaining cellular traction forces at the fluid interface, thereby we have earlier demonstrated successful culturing of human mesenchymal stem cells (hMSCs) and induction of their neuronal differentiation thereon.[12] However, at the same time, this is the trade-off that the robust protein assembly loses original highly deformable nature of the fluid interface and prevents the detection of cellular mechanical work from its deformation.

Here, we developed a highly deformable 2D fluid culture platform that can ideally adapt to cellular morphological and dimensional transitions and quantitatively report mechanical energy mediating the mutual adaptive responses. Our platform is based on a PFCL interface decorated with phospholipid membrane (IPLM) bearing a cell-adhesive peptide and fluorescent tag (Figure 1c). We hypothesized that the bioinert phospholipid coating would prevent protein assembly at the interface, preserving the intrinsically soft and deformable nature of the fluid to adapt and report the mechanical interaction in terms of interfacial strain. Confocal analysis of the IPLM and cells allowed us to visualize the dynamic processes of the interfacial deformation and precise quantification of mechanical energy mediating single-cell adhesion and spreading (Figure 1d). Our platform identified not only unique cellular morphological and energetic dynamics upon interacting with the ultimately adaptive model ECM but also similarity with wetting behaviors of viscous liquid drops, whose details will be discussed below.

2. Results and Discussion

2.1. Development and Characterization of IPLM

Two types of PFCL, Fluorinert FC-40 and FC-70 (Figure S1a, Supporting Information), were used as the bottom layer of the two-phase interfacial culture system (Figure 1c,d). Phospholipids were assembled at the interface by fusing vesicles composed of distearoylphosphatidylcholine (DSPC), RGD-labeled dioleoylphosphatidylethanolamine (DOPE–RGD), and lissamine rhodamine-labeled dioleoylphosphatidylethanolamine (Liss-Rhod-DOPE) at 97.5/2.0/0.5 (mol%) from the upper aqueous layer (Figure S1b,c, Supporting Information). Therefore, the phospholipid-coated interfaces formed are hereafter denoted as IPLM/FC-40 and IPLM/FC-70. At this composition, DSPC defines the entire fluidity of the membranes, whereas DOPE–RGD and Liss-Rhod-DOPE provide cell-binding sites and fluorescent signals to probe interfacial deformation. This interfacial lipid assembly was confirmed by changes in the interfacial tension (I.T.) (Figure S1d, Supporting Information), with values of 38 and

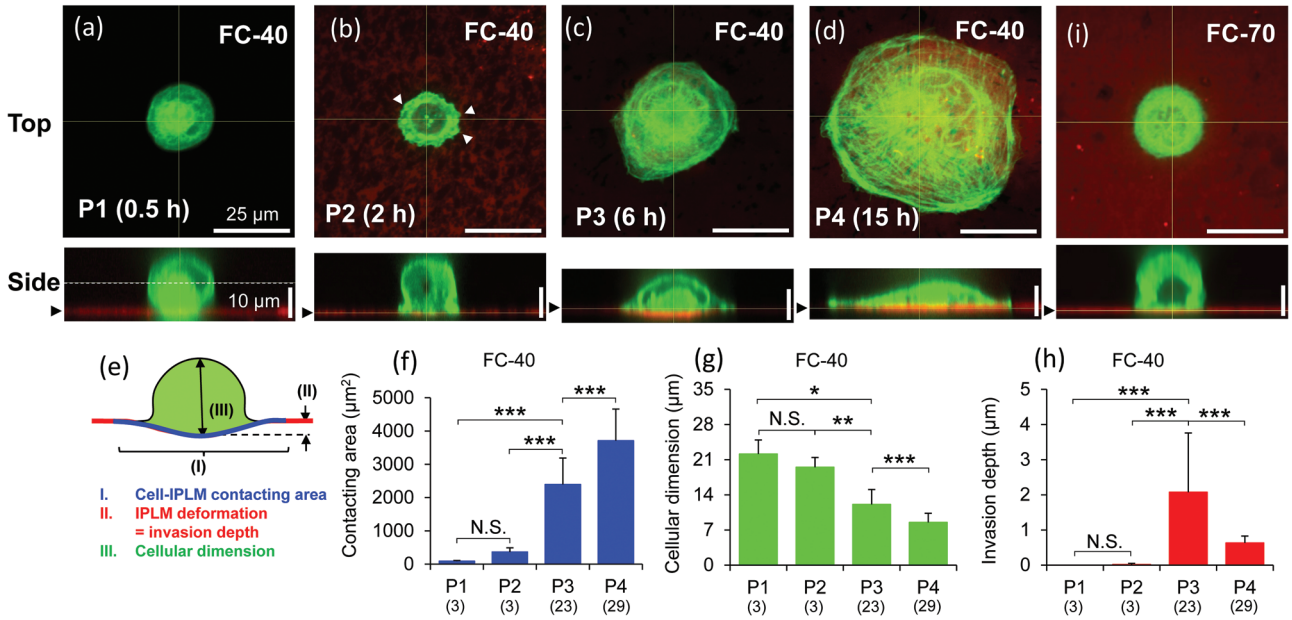

Figure 2. Cellular adaptive wetting. a–d) Representative images of adhesion of MDCK cells expressing LifeAct-GFP to IPLM/FC-40 at given time points: P1, 0.5 h; P2, 2 h; P3, 6 h; P4, 15 h. Green, LifeAct-GFP; Red, rhodamine-labeled lipid. Side views shown below were constructed from stacked confocal images. The arrowheads on the left indicate the water–PFCL interface level. Top views are the cross-section images at the water–PFCL interface and the plane indicated using a white dotted line for (b–d) and (a), respectively. e–h) Quantification of changes in adhesion parameters: (f) cell–IPLM contacting area, (g) cellular dimension, (h) IPLM invasion depth. The number of experiments is shown in parentheses below each bar graph. i) No spreading of the MDCK cell on IPLM/FC-70 with lower I.T. Statistical difference was analyzed by Student's *t*-test: $*p < 0.05$, $**p < 0.01$, $***p < 0.001$.

28 mN m^{-1} for IPLM/FC-40 and IPLM/FC-70, respectively, comparable to previously reported values.[13] Given the high phase transition temperature of DSPC (55 °C), both IPLMs exhibited a laterally nonfluid nature at 37 °C, as evidenced by fluorescence recovery after photobleaching (Figure S2, Supporting Information), which is critical for cell adhesion because traction forces dissipate on less viscous lipid coatings.[14] Moreover, the bioinert nature of the phospholipid layers was verified by the negligible adsorption of fluorescently labeled proteins (Figure S3, Supporting Information). Additionally, in contrast to pristine PFCL, no cell adhesion or spreading was observed for IPLM lacking the RGD ligand, even after fibronectin treatment (Figure S4, Supporting Information). This maintained the intrinsic deformable and adaptive nature of the fluid interfaces, which was mostly lost in our previous fluid interfaces due to the formation of solid-like protein nanolayers via interfacial jamming.[15]

2.2. Visualization of Dynamic Processes of IPLM Deformation and Cellular Morphological Transition

Having confirmed the successful formation of the bioinert IPLM platform, we first investigated whether the fluid interface was soft enough to readout cell mechanical interactions in terms of the interfacial deformation of IPLM toward the vertical direction during the entire cell adhesion and spreading process. Madin–Darby canine kidney (MDCK) cells stably expressing Lifeact-green fluorescent protein (GFP) were seeded on top of the IPLM formed in an in-house developed cell culture chamber (Figure S5, Supporting Information). The 3D structures of the cells and IPLM were reconstructed from the stacked confocal images. To avoid photobleaching of GFP and rhodamine by prolonged imaging, we analyzed the images of different cells and IPLM at 0.5, 2, 6, and 15 h. We chose these specific time points because the cells as well as IPLM exhibit characteristic morphologies and deformations around these time points, even though our cells are heterogenous in terms of cell cycle and Lifeact-GFP expression levels. These observation time points are hereafter denoted as P1–P4.

In the P1 phase, all the cells touched down at the liquid–liquid interface by gravity while maintaining their spherical morphologies; the IPLM remained flat at the interface (**Figure 2a**). In IPLM/FC-40, the cells started to extend protrusions at their edges at P2 (Figure 2b, top view). Interestingly, at the halfway point of cell spreading (P3), the cross-sectional images showed downward IPLM deformation (Figure 2c, side view; magnified image in Figure S6a in the Supporting Information), which almost returned to the original flat form after overnight culture, concomitant with cellular flattening and spreading (Figure 2d, P4; magnified image in Figure S6b in the Supporting Information). Quantitative analysis of adhesion parameters (Figure 2e), including the cell–IPLM contacting area, cellular dimension, and IPLM deformation (invasion depth), depicts the general trend in the cellular adhesion processes. The cell–IPLM contacting area and cell dimension continued to increase and decrease, respectively (Figure 2f,g), whereas IPLM was deformed transiently at P3 and restored close to its original level at P4 (Figure 2h). The downward IPLM indentation at P3 was neither caused by gravity nor their impact upon touching down at the interface, as the cells could not deform the IPLM/FC-70, which had an even lower I.T., and

stopped spreading thereon (Figure 2i). Unsuccessful cell spreading on IPLM/FC-70 was due to smaller mechanical feedback, alike poor cell spreading on extremely soft substrates. In IPLM/FC-40, the cells exerted traction forces, including the out-of-plane component. Earlier studies based on traction force microscopy reported that cells push soft elastic polyacrylamide hydrogels under the nuclear region and pull them obliquely at the cellular edges.[16] However, the IPLM indentation reached up to 2.0 μm, strongly reflecting its extremely compliant nature and suitable for detecting cellular out-of-plane forces (vertical component). In fact, neither the phospholipid-coated glass nor the robust protein nanolayers formed at the pristine PFCL interface were deformed against cell adhesion because of high Young's modulus in the bulk and interface, respectively (Figure S7, Supporting Information). The eventual IPLM restoration at P4 on IPLM/FC-40 might indicate a reduction in vertical traction in the cellular spread morphology (Figure S6, Supporting Information). It is noteworthy that, thanks to the supersoft nature of IPLM, we identified a unique cell-wetting regime which can be called adaptive wetting (Figure 1b), where the substrate exhibited transient deformation during the cellular spreading process. Similar adaptive wetting was observed in the hMSCs and Michigan Cancer Foundation 10A (MCF10A) cells (Figures S8 and S9, Supporting Information), although cellular yield time differed depending on the cell type. These results indicated that adaptive wetting is a general adhesion behavior exhibited by cells at highly compliant fluid interfaces.

2.3. Manipulation of Cell–IPLM Interaction

To further resolve the cellular adaptive wetting phenomenon, we manipulated the cell–IPLM interactions using two different pharmacological treatments. Transforming growth factor-β_1 (TGF-β_1) induces epithelial–mesenchymal transition and increases cellular traction forces and spreading by stabilizing integrin adhesion and accelerating cytoskeletal rearrangements.[17] On the other hand, blebbistatin, a myosin II inhibitor, attenuates cellular traction forces.[18] These treatments had opposite effects on cell–IPLM interaction.

Figure 3a–e,j–l shows the adhesion behaviors of TGF-β_1-treated MDCK cells on IPLM/FC-40 and their quantification results. Due to the reinforced cell–IPLM interaction, the IPLM deformation and cell spreading became larger compared to the untreated control (Figure 3 vs Figure 2). Specifically, significant IPLM deformation was detected at P2, when the cellular dimensions remained unchanged from the beginning (Figure 3k, P1 vs P2), indicating that cells gained large adhesive areas without losing their spherical morphology. This is strikingly different from conventional solid and hydrogel platforms, in which cells can increase their adhesive area only through flattening. Despite the enhanced cell–IPLM interactions, IPLM almost returned to its original level at P4 (Figure 3d,l), suggesting that the cells exhibited an adaptive wetting regime. During this process, actin cytoskeleton changed from cortical distribution to patchy focal-adhesion-like structures, and eventual forming strong basal stress fibers (Figure S10, Supporting Information). Such changes indicate the redistribution as well as an increase of intracellular mechanical stress.

A more striking behavior was observed for IPLM/FC-70 (Figure 3f–i,m–o). Due to the reinforced cell–RGD interaction triggered by TGF-β_1 treatment, the cell extended lamellipodia at P2 (Figure 3g, arrowheads), which were not observed in the non-TGF-β_1-treated counterparts (Figure 2i). Thereafter, it invaded its body almost completely below the original water–PFCL interface level, while maintaining its spherical shape (Figure 3h, P3). Given the highly deformable nature of IPLM/FC-70, the interface is suggested to have flowed faster than the cytoskeletal rearrangement, resulting in an accelerated increase in the cell–IPLM contacting area by the IPLM wrapping around cell body, rather than by cellular deformation. The cellular dimensions became slightly elongated vertically (Figure 3h,n), presumably owing to the exertion of strong elastic forces from almost the entire cellular surface to squeeze the cell body into the aqueous phase. Nevertheless, the cell withdrew most of its body above the lower PFCL layer by P4 (Figure 3i,m,o). At the same time, actin redistributed between cortical and rather homogenous through the P2–P4 state because of cellular adaptive nature (Figure S11, Supporting Information), which are somehow different from those observed on IPLM/FC-40 (Figure S10, Supporting Information). By contrast, the cells treated with blebbistatin entered the final spreading state, bypassing the IPLM deformation step on IPLM/FC-40 and IPLM/FC-70 (Figure S12, Supporting Information), indicating that the IPLM deformation was closely related to the cellular traction forces.

2.4. Quantification of Cellular Mechanical Work

The highly adaptive and deformable IPLM identified a unique cellular wetting regime, where the IPLM deformation became the highest before reaching the final spreading state. During this process, mechanical energy is transferred back and forth between the cell and IPLM. Quantitative discussion of such cellular mechanical work in "living" cell–ECM interaction is one of the major purposes of this study, therefore we next evaluated dynamic changes in the overall mechanical energy transfer between the cells and IPLM during the mutually adaptive responses.

Perfluorocarbon-based fluid microdroplets can quantify cell-driven stress based on morphological changes.[13a] Similarly, our IPLM platform reports the mechanical energy transfer as numbers. Based on the definition of the I.T., the mechanical work (W_c) cell did on the substrate, commonly discussed in terms of total strain energy,[19] can be calculated using the following equation

$$W_c = \sigma \cdot \Delta A \tag{1}$$

where σ and ΔA represent I.T. and increase in the area of the interface between water–PFCL phases, respectively (Figure 1b and Scheme S1 (Supporting Information)). We assumed a constant lipid coating density during observation as the cell-induced IPLM area changes were negligible compared to the total water–PFCL interface area across the culture chamber. In addition, the cellular cortical tension ($\sigma \approx 0.1$–0.6 mN m^{-1})[20] is approximately two orders smaller than that of the IPLM ($\sigma \approx 28$, 38 mN m^{-1}). Therefore, we could use the σ value determined using the pendent drop method (Figure S1d, Supporting Information) in Equation (1).

The values at the final cell spreading state at P4 were 8.4–12 pJ (**Figure** 4a), which were slightly higher than the

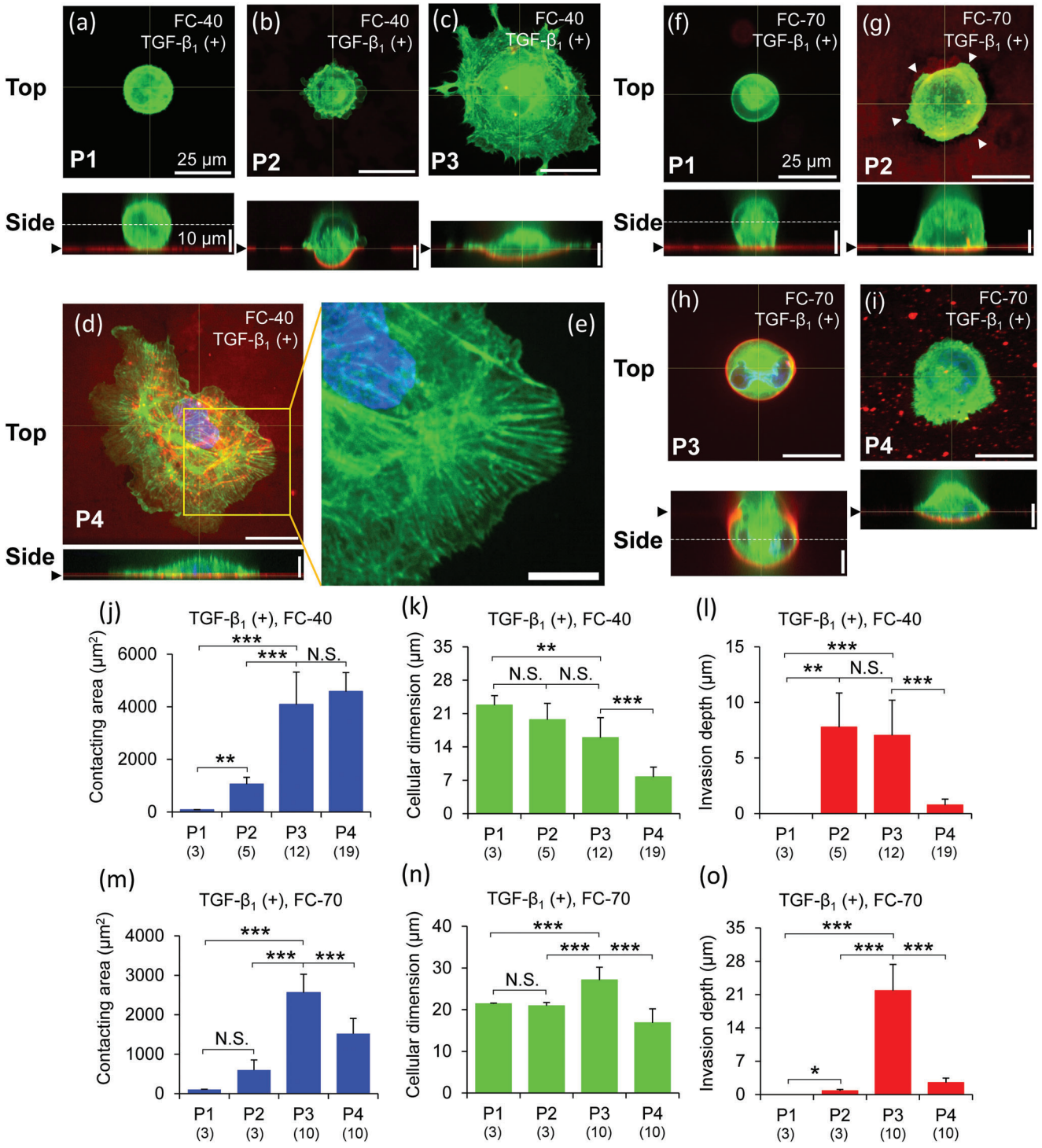

Figure 3. TGF-β_1 reinforces adaptive wetting. a–i) Representative images of adhesion of TGF-β_1-treated MDCK cells to (a–e) IPLM/FC-40 and (f–i) IPLM/FC-70, respectively, at given time points: P1, 0.5 h; P2, 2 h; P3, 6 h; P4, 15 h. Side views were reconstructed from confocal stacked images. The arrowheads in the left indicate the water–PFCL interface level. Top views are the cross-sectional images at the water–PFCL interface for (b–e), (g), and (i), and the planes indicated by white dotted lines from (a), (f), and (h). (e) Magnified image of the indicated region in (d). Arrowheads in (g) represent the lamellipodia. j–o) Changes in the adhesion parameters during adhesion on (j–l) IPLM/FC-40 and (m–o) IPLM/FC-70, respectively. The number of experiments is indicated in parentheses below each bar. Statistical differences were analyzed using Student's *t*-test with statistical differences: $*p < 0.05$, $**p < 0.01$, $***p < 0.001$.

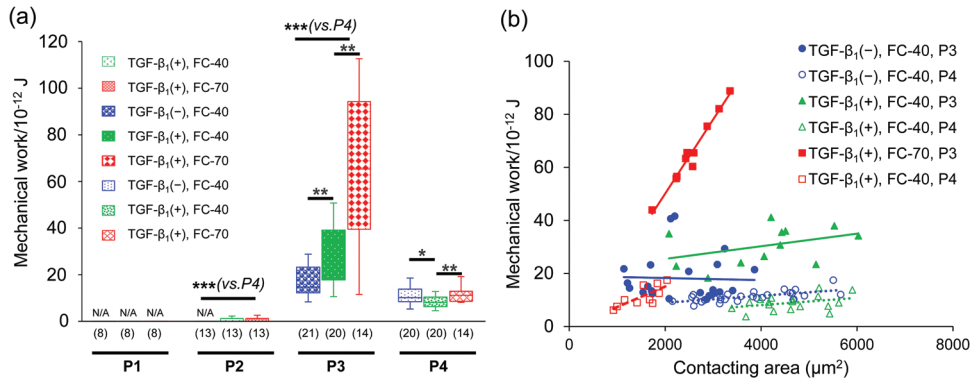

Figure 4. Cell mechanical work analysis. a) Mechanical work quantification by using IPLM. P1–P4 corresponds to 0.5, 2, 6, and 15 h, respectively. The number of experiments is shown in parentheses below each bar graph. N/A represents nondetectable work value. The data were statistically analyzed between different experimental conditions (FC-40 vs FC-70 or TGF-β_1 (+) vs (−)) for the same phases (P2–P4), and for the same conditions against P4. b) The relationship between cellular contacting area and mechanical work at P3 (filled symbols) and P4 (open symbols) for the cells attaching on different IPLMs (FC-40 vs FC-70) and with and without TGF treatment. Cell contacting area is defined as Figure 2e.

total strain energy determined by traction force microscopy[21] and elastic micropillars[22] (10^{-1}–10^{0} pJ), which was reasonable, considering the following two aspects. i) These conventional technologies only calculate in-plane forces (horizontal to the surface), whereas the IPLM can read both in-plane and out-of-plane forces (vertical to the surface). ii) Owing to the extremely soft nature of the fluid IPLM (or by far lower loss modulus than polydimethylsiloxane (PDMS) elastomers), cellular mechanical energy can be efficiently transferred to the IPLM as the viscous dissipation during its deformation is minimized owing to the low viscosity of the interfacial fluids and the deformation speed. Moreover, surprisingly, the work values were higher at P3 than the final P4: 1.7-fold, 3.7-fold, and 5.7-fold for IPLM/FC-40 without TGF-β_1, IPLM/FC-40 with TGF-β_1, and IPLM/FC-70 with TGF-β_1, respectively. Especially, the work exerted by the TGF-β_1-treated cells on the IPLM/FC-70 increased up to 64 ± 31 pJ at the P3 state. Earlier studies on micropillars reported increases in the total strain energy or total force per cell during the spreading processes.[22,23] In addition, other studies reported that the cellular mechanical output did not change regardless of the substrate stiffness; rather, it was mostly governed by the cellular spreading area and the geometry of the adhesion spots.[24] However, in our measurements, the cellular mechanical output was extremely different at the I.T. interfaces (IPLM/FC-40 vs IPLM/FC-70), especially at the P3 stage. This difference became more evident when the cellular work value of each cell was plotted against the cell contact area (defined in Figure 2e), with a significant impact of the cell contact area on the mechanical output only for the TGF-β_1-treated cells on IPLM/FC-70 at the P3 state (Figure 4b, red filled squares), rather moderate cell area dependency on the final P4 state (Figure 4b, red open squares). Therefore, our platform highlighted the unanticipated cellular performance of transiently exerting the highest mechanical energy on their surrounding ECMs depending on the mechanical property underneath.

2.5. Mimicking Cellular Adaptive Wetting Using a Viscous Drop

The above analyses demonstrated unique morphological (Figures 2 and 3) and energetic (Figure 4) transitions upon cell adhesion to fluid IPLM interfaces, which differed from those of conventional solid/hydrogel platforms. To investigate the origin of this gap, a physical experiment was conducted. A drop of linear PDMS liquid, with varied viscosities (μ = 0.01–20 000 Pa s), was hung from a dispenser and gently sunk to the water phase (**Figure 5a**) and the morphological transitions of the PDMS drop and the water–PDMS interface were recorded from the side using a high-speed camera (Figure 5b and Movie S1 (Supporting Information)). Here, the PDMS drop and air–water interface simulate cells and IPLM, respectively. The PDMS was chosen from the following reasons. 1) It is immiscible with water, but due to the surface/interface tension balance, PDMS drops spread on the water pool, resulting in significant contact between PDMS and water. 2) The relaxation time of PDMS increases with the viscosity because of its polymer entanglement complexity without changing its surface tension. Because of the first point (positive spreading constant), the tensional force drives PDMS to spread horizontally against air–water interface, which resembles strong adhesion between cell-surface and RGD-presenting IPLM. In addition, we applied forces to press down and keep the light PDMS drop (d = 0.935–0.979) in the heavier water phase (d = 1.0). This delivers mechanical energy to the system, which substitutes for actomyosin-driven contractility in the case of cell adhesion. However, considering the orthogonal relationship of the force vector against the interfacial tension, the forces exerted by needle will not affect PDMS spreading. Whereas the second point (relaxation time tunability of PDMS) is crucial to simulate the different balances of the adaptation timescales between the cells and the model ECM, either conventional solid/hydrogel or IPLM. The timescale of cellular morphological and dimensional transition is in hours scale, which is different from that of PDMS wetting and shape evolution. Therefore, we defined the contact line relaxation time as the time when the PDMS drop stopped changing shape in water and introduced the Deborah number (De) = [contact line relaxation time]/[observation time] to feature the PDMS shape. This allows us to crosslink the common physical phenomena between cellular spreading and PDMS wetting.

Because of the effects of capillary, the least viscous PDMS drop (μ = 0.01 Pa s) rapidly spreads the air–water interface from the beginning of the interaction, indicating negligibly short relaxation

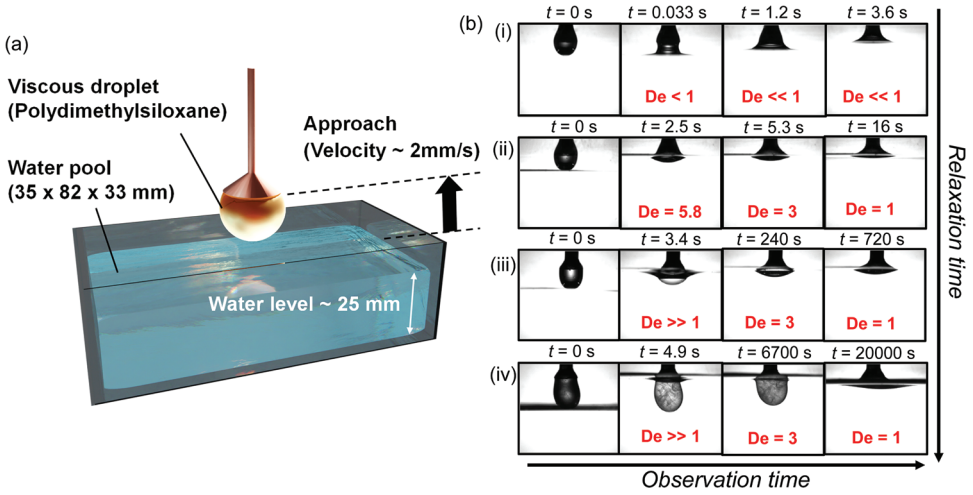

Figure 5. Physical model. a) Schematic drawing of the experiment, where PDMS drops with different viscosities were pressed to the air–water interface. b) Time-lapse images of PDMS–water interface for i) 0.01, ii) 5, iii) 100, iv) 20 000 Pa s drops cropped from Movie S1 (Supporting Information). The Deborah numbers (De) were calculated from the observation time (t) and the relaxation time (τ) of each drop: i) <0.033, ii) 16, iii) 720, iv) 20 000 s. It is defined as the contact line relaxation time when the interface of water and each drop stops the morphological change.

time (Figure 5b(i)). Thus, De << 1 throughout the observational period, and PDMS exhibits fluid behaviors. However, with increasing viscosity, the initial indentation of the PDMS–water interface became larger with less deformation of the PDMS drop (Figure 5b(ii)–(iv), 2nd photos). In other words, by manipulating the adaptation timescales balance between water and PDMS, we are able to see increases in De at this time point, making the PDMS drops more elastic or viscoelastic. Over time, the viscous drops gradually deformed and completed the morphological transition (De = 1). Analysis of a series of drops revealed that the dominant regulation of the degree of maximum interfacial deformation, and thereby mechanical energy transfer as well, by the PDMS relaxation time was due to the constant interfacial tension of the PDMS drops. When we compared these results with the cellular behavior at the IPLM interfaces, cellular adaptive wetting became apparent by remaining the original deformable nature of the fluid interface by lipid coating, highlighting overall viscoelastic nature of cell body. Under these circumstances, pharmacological treatments and using different PFCLs manipulated the balance of the adaptation timescales between the cells and substrates, altering the maximum mechanical energy transfer from the cell to the IPLM, thereby we were able to see unique time-dependent morphological and energetic transition behaviors at the fluid interfaces.

3. Conclusion

We demonstrate here "living" cell–fluid interfaces, which can ideally adapt to cellular morphological and dimensional transition to probe mechanical interaction therein. The phospholipid coating at the interface prevents the formation of solid-like protein nanolayers, thereby remaining the original deformable and adaptive nature. On conventional solid surfaces, cells can only enlarge their adhesion area by changing their morphology to adapt to the substrate (cell flattening; Movie S2, Supporting Information). While, on the IPLM, cells do not necessarily have to remodel their body shape as the support interface is highly deformable. Therefore, IPLM deformation precedes cellular deformation (Movie S3, Supporting Information), implying that the cells and ECM could interact more rapidly; however, the slow relaxation time of the cellular morphological transition, as well as the poorly adaptive nature of the ECM, hampers this process in conventional cell culture setups. By making the fluid interface more deformable and adaptive, we successfully identified a new cellular wetting regime in which the IPLM deforms first, followed by its restoration and cellular flattening (Figures 2 and 3). Such sequential and alternative deformation of matter across the interface could be mimicked by using simple experiments on the wetting of PDMS drops on the air–water interface (Figure 5), further suggesting a deep relationship between cellular mechanics and wetting. In the physics of wetting on surfaces with a low Young's modulus must consider time-dependent interfacial shape changes, sometimes denoted as soft or adaptive wetting, which is still debated.[25] Thus, cell mechanics can potentially be modeled in similar adaptive wetting scenarios.[26]

Furthermore, quantifying the mechanical work exerted by the cells on the IPLM, or the total strain energy, allowed us to link cellular wetting morphology and their mechanical interactions with their surroundings. Depending on the pharmacological treatment (TGF-β_1 and blebbistatin) as well as the steps during cell spreading, the strain energy changes drastically (Figure 4). In particular at the P3 stage, the mechanical work reached its highest levels, which were almost one order of magnitude larger than those reported for the conventional solid/hydrogel platforms, implying that cells have a much higher potential to transfer mechanical energy to their surroundings than expected. Successful identification of this unanticipatedly high cellular mechanical performance, even though transient, is important because cellular structures and functions depend on mechanical hysteresis[27] and the substrate strain energy.[28] Moreover, in the P3 phase for the TGF-β_1-treated cells on IPLM/FC-70 (Figure 3h), the RGD ligands are presented to almost the entire surface of the cells. Considering the cellular capability to autonomously generate such a high-strain energy state as well as its quasi-3D nature, the IPLM

platform will provide ultimate "livingness" beyond conventional adaptive biomaterials and aid in the manipulation of cellular fates for tissue engineering and regenerative medicine.

Supporting Information

Supporting Information is available from the Wiley Online Library or from the author.

Acknowledgements

This study was supported in part by the Japan Society for the Promotion of Science, KAKENHI (Grant No. 21H01643 to M.T., and Grant Nos. 22H00596 and 23K17481 to J.N.).

Conflict of Interest

The authors declare no conflict of interest.

Data Availability Statement

The data that support the findings of this study are available from the corresponding author upon reasonable request.

Keywords

cell adhesion, fluid, mechanobiology, viscoelasticity, wetting

Received: March 6, 2024
Published online: April 29, 2024

[1] A. Walther, *Adv. Mater.* **2020**, *32*, 1905111.
[2] a) T. Iskratsch, H. Wolfenson, M. P. Sheetz, *Nat. Rev. Mol. Cell Biol.* **2014**, *15*, 825; b) E. E. Charrier, K. Pogoda, R. G. Wells, P. A. Janmey, *Nat. Commun.* **2018**, *9*, 449.
[3] A. P. Liu, E. A. Appel, P. D. Ashby, B. M. Baker, E. Franco, L. Gu, K. Haynes, N. S. Joshi, A. M. Kloxin, P. H. J. Kouwer, J. Mittal, L. Morsut, V. Noireaux, S. Parekh, R. Schulman, S. K. Y. Tang, M. T. Valentine, S. L. Vega, W. Weber, N. Stephanopoulos, O. Chaudhuri, *Nat. Mater.* **2022**, *21*, 390.
[4] a) C. E. Chan, D. J. Odde, *Science* **2008**, *322*, 1687; b) A. Elosegui-Artola, X. Trepat, P. Roca-Cusachs, *Trends Cell Biol.* **2018**, *28*, 356.
[5] a) O. Chaudhuri, L. Gu, M. Darnell, D. Klumpers, S. A. Bencherif, J. C. Weaver, N. Huebsch, D. J. Mooney, *Nat. Commun.* **2015**, *6*, 7365; b) O. Chaudhuri, L. Gu, D. Klumpers, M. Darnell, S. A. Bencherif, J. C. Weaver, N. Huebsch, H.-p. Lee, E. Lippens, G. N. Duda, D. J. Mooney, *Nat. Mater.* **2016**, *15*, 326.
[6] Z. Gong, S. E. Szczesny, S. R. Caliari, E. E. Charrier, O. Chaudhuri, X. Cao, Y. Lin, R. L. Mauck, P. A. Janmey, J. A. Burdick, V. B. Shenoy, *Proc. Natl. Acad. Sci. USA* **2018**, *115*, E2686.
[7] D. Gonzalez-Rodriguez, K. Guevorkian, S. Douezan, F. Brochard-Wyart, *Science* **2012**, *338*, 910.
[8] C. Pérez-González, R. Alert, C. Blanch-Mercader, M. Gómez-González, T. Kolodziej, E. Bazellieres, J. Casademunt, X. Trepat, *Nat. Phys.* **2019**, *15*, 79.
[9] a) U. S. Schwarz, J. R. D. Soiné, *Biochim. Biophys. Acta* **2015**, *1853*, 3095; b) J. L. Tan, J. Tien, D. M. Pirone, D. S. Gray, K. Bhadriraju, C. S. Chen, *Proc. Natl. Acad. Sci. USA* **2003**, *100*, 1484; c) J. Fu, Y.-K. Wang, M. T. Yang, R. A. Desai, X. Yu, Z. Liu, C. S. Chen, *Nat. Methods* **2010**, *7*, 733; d) R. W. Style, R. Boltyanskiy, G. K. German, C. Hyland, C. W. MacMinn, A. F. Mertz, L. A. Wilen, Y. Xu, E. R. Dufresne, *Soft Matter* **2014**, *10*, 4047; e) W. R. Legant, C. K. Choi, J. S. Miller, L. Shao, L. Gao, E. Betzig, C. S. Chen, *Proc. Natl. Acad. Sci. USA* **2013**, *110*, 881; f) H. Colin-York, D. Shrestha, J. H. Felce, D. Waithe, E. Moeendarbary, S. J. Davis, C. Eggeling, M. Fritzsche, *Nano Lett.* **2016**, *16*, 2633.
[10] a) C. Grashoff, B. D. Hoffman, M. D. Brenner, R. Zhou, M. Parsons, M. T. Yang, M. A. McLean, S. G. Sligar, C. S. Chen, T. Ha, M. A. Schwartz, *Nature* **2010**, *466*, 263; b) D. R. Stabley, C. Jurchenko, S. S. Marshall, K. S. Salaita, *Nat. Methods* **2012**, *9*, 64; c) Y. Zhang, C. Ge, C. Zhu, K. Salaita, *Nat. Commun.* **2014**, *5*, 5167; d) M. Iwaki, S. F. Wickham, K. Ikezaki, T. Yanagida, W. M. Shih, *Nat. Commun.* **2016**, *7*, 13715.
[11] a) D. Kong, K. D. Q. Nguyen, W. Megone, L. Peng, J. E. Gautrot, *Faraday Discuss.* **2017**, *204*, 367; b) D. Kong, W. Megone, K. D. Q. Nguyen, S. Di Cio, M. Ramstedt, J. E. Gautrot, *Nano Lett.* **2018**, *18*, 1946.
[12] a) X. Jia, K. Minami, K. Uto, A. C. Chang, J. P. Hill, J. Nakanishi, K. Ariga, *Adv. Mater.* **2020**, *32*, 1905942; b) X. Jia, J. Song, W. Lv, J. P. Hill, J. Nakanishi, K. Ariga, *Nat. Commun.* **2022**, *13*, 3110.
[13] a) O. Campas, T. Mammoto, S. Hasso, R. A. Sperling, D. O'Connell, A. G. Bischof, R. Maas, D. A. Weitz, L. Mahadevan, D. E. Ingber, *Nat. Methods* **2014**, *11*, 183; b) K. Ullmann, L. Poggemann, H. Nirschl, G. Leneweit, *Colloid Polym. Sci.* **2020**, *298*, 407.
[14] M. Bennett, M. Cantini, J. Reboud, J. M. Cooper, P. Roca-Cusachs, M. Salmeron-Sanchez, *Proc. Natl. Acad. Sci. USA* **2018**, *115*, 1192.
[15] X. Jia, K. Minami, K. Uto, A. C. Chang, J. P. Hill, T. Ueki, J. Nakanishi, K. Ariga, *Small* **2019**, *15*, 1804640.
[16] a) H. Delanoë-Ayari, J. P. Rieu, M. Sano, *Phys. Rev. Lett.* **2010**, *105*, 248103; b) S. S. Hur, Y. Zhao, Y.-S. Li, E. Botvinick, S. Chien, *Cell. Mol. Bioeng.* **2009**, *2*, 425.
[17] A. H. Mekhdjian, F. Kai, M. G. Rubashkin, L. S. Prahl, L. M. Przybyla, A. L. McGregor, E. S. Bell, J. M. Barnes, C. C. DuFort, G. Ou, A. C. Chang, L. Cassereau, S. J. Tan, M. W. Pickup, J. N. Lakins, X. Ye, M. W. Davidson, J. Lammerding, D. J. Odde, A. R. Dunn, V. M. Weaver, *Mol. Biol. Cell* **2017**, *28*, 1467.
[18] K. Yamamoto, H. Miura, M. Ishida, Y. Mii, N. Kinoshita, S. Takada, N. Ueno, S. Sawai, Y. Kondo, K. Aoki, *Nat. Commun.* **2021**, *12*, 7145.
[19] J. P. Butler, I. M. Tolić-Nørrelykke, B. Fabry, J. J. Fredberg, *Am. J. Physiol.: Cell Physiol.* **2002**, *282*, C595.
[20] D. Schneider, T. Baronsky, A. Pietuch, J. Rother, M. Oelkers, D. Fichtner, D. Wedlich, A. Janshoff, *PLoS One* **2013**, *8*, e80068.
[21] T. Mizutani, K. Furusawa, H. Haga, K. Kawabata, *Regener. Ther.* **2016**, *3*, 90.
[22] J. Foolen, J.-Y. Shiu, M. Mitsi, Y. Zhang, C. S. Chen, V. Vogel, *PLoS One* **2016**, *11*, e0160369.
[23] C. A. Lemmon, C. S. Chen, L. H. Romer, *Biophys. J.* **2009**, *96*, 729.
[24] a) P. W. Oakes, S. Banerjee, M. C. Marchetti, M. L. Gardel, *Biophys. J.* **2014**, *107*, 825; b) G. Yalak, J.-Y. Shiu, I. Schoen, M. Mitsi, V. Vogel, *PLoS One* **2019**, *14*, e0218893; c) A. Ghagre, A. Amini, L. Srivastava, P. Tirgar, A. Khavari, N. Koushki, A. Ehrlicher, *ACS Appl. Mater. Interfaces* **2021**, *13*, 19726; d) T. Andersen, D. Wörthmüller, D. Probst, I. Wang, P. Moreau, V. Fitzpatrick, T. Boudou, U. S. Schwarz, M. Balland, *Biophys. J.* **2023**, *122*, 684.
[25] a) L. Chen, E. Bonaccurso, T. Gambaryan-Roisman, V. Starov, N. Koursari, Y. Zhao, *Curr. Opin. Colloid Interface Sci.* **2018**, *36*, 46; b) S. Karpitschka, S. Das, M. van Gorcum, H. Perrin, B. Andreotti, J. H. Snoeijer, *Nat. Commun.* **2015**, *6*, 7891; c) L. A. Lubbers, J. H. Weijs, L. Botto, S. Das, B. Andreotti, J. H. Snoeijer, *J. Fluid Mech.* **2014**, *747*, R1; d) H.-H. Tran, D. Lee, D. Riassetto, *Rep. Prog. Phys.* **2023**, *86*, 066601.
[26] H.-J. Butt, R. Berger, W. Steffen, D. Vollmer, S. A. L. Weber, *Langmuir* **2018**, *34*, 11292.
[27] a) C. Yang, M. W. Tibbitt, L. Basta, K. S. Anseth, *Nat. Mater.* **2014**, *13*, 645; b) L. Yu, Y. Hou, W. Xie, J. L. Cuellar-Camacho, Q. Wei, R. Haag, *Adv. Mater.* **2020**, *32*, 2006986.
[28] V. Panzetta, S. Fusco, P. A. Netti, *Proc. Natl. Acad. Sci. USA* **2019**, *116*, 22004.